Structural Characterization of Mixed $(TiO_2)_x(ZrO_2)_y(SiO_2)_{1-x-y}$ Sol−Gels ($0.05 \leq x, y \leq 0.15$) by a Combination of X-ray and Spectroscopy Techniques

Gavin Mountjoy,*,† Mark A. Holland,† Graham W. Wallidge,‡ Philips Gunawidjaja,‡ Mark E. Smith,‡ David M. Pickup,† and Robert J. Newport†

School of Physical Sciences, University of Kent, Canterbury, Kent, United Kingdom, CT2 7NR, and Physics Department, University of Warwick, Coventry, United Kingdom, CV4 7AL

Received: October 14, 2002; In Final Form: April 25, 2003

A combination of extended X-ray absorption fine structure (EXAFS), X-ray absorption near-edge structure (XANES), Fourier transform infrared (FTIR), and ^{17}O nuclear magnetic resonance (NMR) spectroscopies, small-angle X-ray scattering (SAXS), and X-ray diffraction (XRD) has been used to study the atomic structure of $(TiO_2)_x(ZrO_2)_y(SiO_2)_{1-x-y}$ xerogels ($0.05 \leq x, y \leq 0.15$). The samples were prepared by reacting Ti butoxide and Zr *n*-propoxide with acetylacetone, to reduce reactivity of the metal alkoxides, and then reacting with partially hydrolyzed tetraethyl orthosilicate. EXAFS and XANES results imply that simultaneous insertion of Zr and Ti oxides into a silica host network causes the metals to adopt environments similar to those observed for the corresponding binary Zr oxide− and Ti oxide−silica systems. XANES, SAXS, and XRD indicate that the samples with up to 20 mol % total metal loading remain homogeneous with heat treatment up to 500 °C. ^{17}O NMR indicates that both Ti- and Zr-rich samples with 20 mol % total metal loading exhibit phase separation after heat treatment at 750 °C. After heat treatment at 1000 °C, the sample with $x = 0.15$ and $y = 0.05$ shows clear evidence from XRD of phase separation in the form of $ZrTiO_4$ domains, which is not seen in other samples.

1. Introduction

Glass formation by the sol−gel process allows the production of TiO_2–ZrO_2–SiO_2 systems, which have a number of interesting properties. The TiO_2 content can be varied to control the refractive index to desired values,[1] while the thermal expansion coefficient can be favorably changed to approach zero. Increased chemical durability can also be achieved, especially against alkaline solutions, by altering the ZrO_2 content.[2]

Glasses of the TiO_2–ZrO_2–SiO_2 system are difficult to produce by conventional melt−quench techniques due to the elevated temperatures that are required during production. This causes these multicomponent systems to be very susceptible to phase separation. (In this report, phase separation does not denote a thermodynamic transition but refers to the appearance of regions with metal oxide composition.) The sol−gel process is therefore preferred since homogeneous samples can be prepared at much lower temperatures within a relatively short time frame (i.e., days). Sol−gel processing also facilitates specialist applications such as those requiring thin films or membranes.[3]

Our group has previously undertaken extensive characterization of binary $(ZrO_2)_y(SiO_2)_{1-y}$ [e.g., 4,5] and $(TiO_2)_x(SiO_2)_{1-x}$ [e.g., 6,7] xerogel samples, in particular focusing on the local atomic environment of the metal atoms. There have been few studies of the ternary TiO_2–ZrO_2–SiO_2 system in comparison to the binary systems.[2,8,9] In addition, those studies have not addressed the atomic structure of the materials obtained. Here we examine whether the metal atom environments in TiO_2–ZrO_2–SiO_2 samples are the same as those in previously studied binary systems.

This study was achieved primarily through EXAFS (extended X-ray absorption fine structure) and XANES (X-ray absorption near-edge structure) spectroscopies and ^{17}O NMR (nuclear magnetic resonance) spectroscopy, which give complementary details on the local environments of the Ti and Zr metal sites within the silica matrix. We also present FTIR (Fourier transform infrared spectroscopy), XRD (X-ray diffraction), and SAXS (small-angle X-ray scattering) results to provide additional insight into the effects of inserting two metal atoms into the silica matrix: XRD is particularly suited to showing changes in the overall amorphous network, while SAXS offers information on changes in homogeneity.

2. Methods and Data Analysis

2.1. Sample Preparation. The synthesis of the TiO_2–ZrO_2–SiO_2 xerogels is based upon a method[2,8] in which the main goal is to obtain homogeneous samples, i.e., with a high degree of atomic dispersion of Ti and Zr atoms in the silica matrix. This was primarily achieved by using the organic modifier acetylacetone (acac; Fluka, 99.5%), which allows control of the reactivity of the Ti and Zr alkoxides by the formation of larger, slower-reacting molecules by ligand exchange. The following precursors were used in the sol−gel process: tetraethyl orthosilicate, TEOS (Aldrich, 98%); Zr(IV) *n*-propoxide, $Zr(OPr^n)_4$

* Corresponding author.
† University of Kent. Fax +441227827558; e-mail g.mountjoy@ukc.ac.uk (G.M.), d.m.pickup@ukc.ac.uk (D.M.P.), r.j.newport@ukc.ac.uk (R.J.N.).
‡ University of Warwick. Fax +442476692016; e-mail g.w.wallidge@rl.ac.uk (G.W.W.), phrzh@warwick.ac.uk (P.G.), m.e.smith.1@warwick.ac.uk (M.E.S.).

10.1021/jp022225x CCC: $25.00
Published on Web 07/02/2003

TABLE 1: Zr K-Edge and Ti K-Edge EXAFS Fits to Reference Samples[a]

	crystallographic data			experimental EXAFS results		
reference sample	shell	N_{R-O}	R_{R-O}/Å	R_{R-O}/Å	$2\sigma^2$/Å^2	R_{dis}/%
anatase[34]	Ti−O	6	1.94	1.96 (0.01)	0.010 (0.001)	39
	Ti−Ti	4	3.04	3.06 (0.02)	0.006 (0.002)	
	Ti−Ti	4	3.79	3.86 (0.02)	0.005 (0.002)	
	Ti−O	8	3.86	3.92 (0.03)	0.008 (0.003)	
$ZrTiO_4$[31] (Ti K-edge)	Ti−O_a	4	2.00	1.89 (0.01)	0.027 (0.001)	45
	Ti−O_b	2	2.20	2.44 (0.01)	0.016 (0.001)	
	Ti−Zr	6	3.60	3.63 (0.02)	0.024 (0.002)	
	Ti−Ti	6	3.60	3.56 (0.03)	0.039 (0.003)	
$ZrSiO_4$[35]	Zr−O_a	4	2.13	2.13 (0.01)	0.006 (0.001)	48
	Zr−O_b	4	2.27	2.23 (0.01)	0.002 (0.002)	
	Zr−Si	2	2.99	2.99 (0.02)	0.011 (0.002)	
	Zr−Zr	4	3.63	3.63 (0.03)	0.007 (0.002)	
t-ZrO_2[36]	Zr−O_a	4	2.08	2.09 (0.01)	0.010 (0.001)	39
	Zr−O_b	4	2.38	2.28 (0.03)	0.046 (0.015)	
	Zr−Zr	12	3.62	3.62 (0.01)	0.018 (0.001)	
m-ZrO_2[36]	Zr−O	7	2.16	2.14 (0.01)	0.016 (0.001)	36
	Zr−Zr_a	7	3.45	3.46 (0.02)	0.014 (0.002)	
	Zr−Zr_b	4	3.98	3.99 (0.03)	0.016 (0.002)	
$ZrTiO_4$[31] (Zr K-edge)	Zr−O_a	4	2.00	2.06 (0.01)	0.006 (0.001)	35
	Zr−O_b	2	2.20	2.20 (0.01)	0.003 (0.002)	
	Zr−Ti	6	3.60	3.60 (0.02)	0.066 (0.002)	
	Zr−Zr	6	3.60	3.56 (0.03)	0.042 (0.002)	
$BaZrO_3$[37]	Zr−O	6	2.09	2.09 (0.01)	0.005 (0.001)	46
	Zr−Ba	8	3.62	3.62 (0.02)	0.020 (0.002)	
	Zr−Zr	6	4.18	4.24 (0.02)	0.002 (0.002)	

[a] Errors are shown in parentheses. R_{dis} is the "goodness of fit", defined in eq 2. References are for crystallographic data. EXAFS data for t-ZrO_2 are from our previous work.[4]

(70 wt % solution in propan-1-ol, Aldrich); and Ti butoxide, $Ti(OBu^i)_4$ (Alfa, 99%). HCl (Fisons) was used as a catalyst and ethanol (Aldrich) was used as a mutual solvent. In this method, the modified alkoxides are mixed in the order of their reactivities, i.e., TEOS, followed by Ti butoxide, followed by Zr propoxide. After a typical gelation time of 3−4 days, the resultant xerogels were aged for a further 7 days. All the samples were then air-dried for several days, finely ground, and then dried under vacuum for 24 h to remove any excess solvent. Heat treatments up to 750 °C were performed at 2 °C min^{-1} with target temperature maintained for 2 h.

The TiO_2 and ZrO_2 contents were varied between 5 and 15 mol %, with a total metal content of not greater than 20 mol %. For the remainder of this paper the following nomenclature will be introduced to simplify sample identification. For example, the composition $ZrO_2-TiO_2-SiO_2$ of 5:15:80 that has been heat-treated to 500 °C will be referred to as Zr5/Ti15(500).

2.2. EXAFS and XANES Experimental. Ti and Zr K-edge absorption spectra were collected on stations 8.1 and 9.2 at the Daresbury Laboratory SRS, Daresbury, U.K., by use of Si [111] and [220] crystal monochromators, respectively. Samples with a suitable optical thickness and high uniformity were prepared for the experiments by grinding and diluting in polyethylene. Standard ionization chambers were placed in the beam path before and after the sample to measure incident and transmitted intensities. Spectra were collected at the Ti K-edge (4966 eV) and the Zr K-edge (17998 eV) in transmission mode at room temperature. Harmonic contaminants were removed from the beam via 50% harmonic rejection. EXAFS and XANES data were collected simultaneously and were typically summed across three separate scans. Ti and Zr metal foils were placed in front of a third ion chamber, which was used for energy calibration.

2.3. EXAFS Data Analysis. The programs EXCALIB and EXBROOK were used to reduce the EXAFS data. The EXAFS data are analyzed to obtain the absorbance, $\mu t = \ln(I_t/I_0)$, and then normalized absorbance $\chi(k) = (\mu t(k) - \mu t_{pre})/(\mu t_{post} - \mu t_{pre})$, where k is the photoelectron wave vector. The program EXCURV98 was used to fit the EXAFS spectra, by use of the curved wave, single scattering equation:[10]

$$\chi(k) = AFAC\sum \frac{N_j}{kR_j^2} |f(\pi, k, R_j)| e^{-2R_j/\lambda(k)} e^{-2\sigma_j^2 k^2} \sin[2kR_j + 2\delta(k) + \psi(k,R_j)] \quad (1)$$

AFAC is the proportion of electrons that undergo an EXAFS-type scatter. N_j is the coordination number, and R_j is the interatomic distance for the jth shell. The Debye−Waller factor is $A_j = 2\sigma_j^2$. $\delta(k)$ and $\psi(k, R_j)$ are the phase shifts experienced by the photoelectron, $f(\pi, k, R_j)$ is the amplitude of the photoelectron backscattering, and $\lambda(k)$ is the electron mean free path. EXCURV98 uses an additional parameter, E_F, to correct the edge position. Equation 1 does not include the effects of multiple scattering. Fortunately, multiple scattering is less significant for amorphous materials and will not affect results for Zr−O and Ti−O correlations.

Least-squares refinements of the structural parameters of our samples were carried out against the k^3-weighted $\chi(k)$ in k-space. Values of $k_{min} = 3.7$ and $k_{max} \sim 13$ Å^{-1} were used for the Zr K-edge data, while values of $k_{min} = 3.6$ and $k_{max} \sim 11$ Å^{-1} were used for the Ti K-edge. It has been reported that Zr K-edge EXAFS oscillations are sometimes affected by the presence of a double-electron transition at ~7.7 Å^{-1}.[11] The data collected here, however, did not show a significant feature at this point; thus the double-electron excitation was ignored during data analysis.

Fits to the reference samples (as listed in Table 1) were carried out to check the accuracy of the phase shifts and to determine

values of *AFAC*. The values of AFAC were obtained by using values of N_j and R_j from crystallographic data and then allowing the variables R_j, E_F, $2\delta^2$, and *AFAC* to vary until the best fit was achieved. This resulted in *AFAC* being set at 0.85 and 0.80 for the Zr and Ti K-edge data sets, respectively. The results of the refinements are reported in terms of the discrepancy index:

$$R_{dis} = \frac{\sum_i k_i^3 |\chi(k_i)_{expt} - \chi(k_i)_{fit}|}{\sum_i k_i^3 |\chi(k_i)_{expt}|} \times 100 \qquad (2)$$

The statistical fit error and uncertainties are calculated within EXCURV98. The overall errors values are likely to be greater due to sources of inaccuracy beyond fit statistics, such as the quality of the background subtraction. Reasonable estimates of the total errors are ±0.02 Å for nearest-neighbor separations and ±20% for nearest-neighbor coordinations.

2.4. XANES Data Analysis. The XANES spectra were processed according to earlier work[7] to obtain the normalized absorbance. XANES spectra for transition metal oxides show characteristic features,[12] with the preedge peak(s) corresponding to 1s to nd transitions with p−d mixing.[13] Such transitions are not allowed for completely centrosymmetric metal atom sites, but the preedge peak intensity increases as the degree of centrosymmetry decreases. The shape of the main absorption peak represents transitions to np continuum states and "shape resonances" of the metal atom environment.[12] Qualitative information can be obtained by comparing XANES spectra with those of reference compounds (the so-called "fingerprint" method) [e.g., ref 5]. Farges et al.[14,15] have shown that reliable information about Ti coordination can be obtained from the position and height of the dominant preedge peak, and we have previously applied this method to TiO_2–SiO_2 xerogels.[7,16]

2.5. SAXS. SAXS spectra were collected on station 8.2 at the Daresbury Laboratory SRS, Daresbury, U.K. X-rays of wavelength $\lambda = 1.54$ Å were used, with four sets of collimating slits to reduce slit scattering. Samples were contained in cells with Kapton windows. Incident and transmitted X-ray intensities were measured in standard ion chambers before and after the sample (respectively). The SAXS intensity was recorded with a quadrant detector. A camera length of 3.5 m was used. The angular scale for SAXS was calibrated from a reference sample of wet rat tail collagen.

Data analysis was undertaken as per previous work,[17] in which the raw data was divided by the detector response function and normalized to the incident beam flux and counting time. The adsorption correction was simplified by using the small-angle approximation ($2\theta \sim 0$), i.e., assuming no path length variation. A background measurement of the empty container was subtracted. An approximate correction for variations in thickness between samples was made by multiplying $I_S(Q)$ by the factor $(\mu_s t_s)^{-1}$, where μ_s is the linear absorption coefficient and t_s is the sample thickness.

2.6. FTIR. IR spectra were recorded in diffuse reflectance mode on a Bio-Rad FT205C spectrometer controlled by Win-IR software. Samples were diluted (1:10 by weight) in dry KBr and scanned in the range 4000−400 cm^{-1} with a resolution of 4 cm^{-1}. Each spectrum was the result of averaging 64 scans. IR spectral assignments were made according to the literature.[18−20] The band at 3590 cm^{-1} is attributed to stretching vibrations involving Si−OH groups, and the broad band at 3350 cm^{-1} corresponds to stretching modes in absorbed water. The band at 1610 cm^{-1} is assigned to the H−O−H bending vibration.

The main region of interest lies between 1450 and 650 cm^{-1} as the peaks observed here are characteristic of a silica-based network. The positions and assignments of these vibrations are as follows: (i) the 800−810 cm^{-1} band is associated with the symmetric ν(Si−O−Si) stretching vibration,[18,20] (ii) the 940−960 cm^{-1} band is best attributed to the stretching vibration of SiO^- groups[20] adjacent to different counterions (in this case, this band has contributions from Ti−O−Si, Zr−O−Si, and Si−OH), (iii) the 1080−1105 cm^{-1} arises from the LO component of asymmetric ν(Si−O−Si) stretching vibrations,[18,20] and (iv) the 1180−1220 cm^{-1} band is associated with the TO component.[18] Additional peaks occur for the nonheated samples: the sharp weak bands at ca. 2900 and 1450 cm^{-1} are due to C−H stretching and bending vibrations, respectively, and other bands at 1600, 1530, 1360, and 1280 cm^{-1} are attributed to stretching and bending vibrations from organic materials remaining in the samples.

2.7. ^{17}O MAS NMR. The ^{17}O magic-angle spinning (MAS) NMR spectra were acquired on a Chemagnetics CMX300 Infinity spectrometer. The spectra were collected at 40.7 MHz under MAS at typically 12.1 kHz, with a recycle delay of 1−2.5 s, using a Chemagnetics 4 mm double-bearing probe. A 90°−τ∠180° echo sequence was applied with a τ-delay of 1 rotor period (66 μs) to overcome the problems of probe ringing, thereby allowing the spectra to be phased correctly. The spectra were referenced externally to H_2O (0 ppm). Typically each spectrum was the result of ∼10^5 coadded scans and took ca. 24 h to collect.

It should be noted that ^{17}O-enriched samples were heated under nitrogen and not air. Heating under the inert atmosphere preserves the ^{17}O labeling, allowing spectra to be accumulated with a better signal-to-noise ratio in a given time. In a separate study,[21] NMR was used to compare the structure of a sample heated under air with that of the same sample heated under an inert atmosphere. ^{29}Si MAS NMR showed the silicate network was effectively the same as revealed by the Q^n speciation. The use of ^{1}H and ^{13}C NMR showed that organic fragments were removed under both atmospheres but at ∼20 °C higher temperature under the inert atmosphere. These NMR data[21] indicate that comparison of samples heated under these different atmospheres is valid.

The NMR spectra are dominated by a central peak, with an isotropic chemical shift at ca. 0 ppm, and shows structure at negative shift due to a second-order quadrupole interaction.[22] The central peak is assigned to Si−O−Si linkages, with a contribution from Si−OH groups;[23] this resonance has spinning side bands at ca. −250 and 265 ppm. In crystalline samples ^{17}O signals from Si−O−Ti linkages are observed at 190 ppm in the mineral fresnoite ($Ba_2TiSi_2O_8$)[24] and 160 ppm in titanite ($CaTiSiO_5$),[25] at 157 ppm in Li_2TiSiO_5,[26] and at 370−295 ppm in cyclic titanodiphenylsiloxanes.[27] Also, Zr−O−Si linkages have been observed at 150 ppm in crystalline zircon.[28] Hence, the signals in gels seen between 110 and 250 ppm are attributed to M−O−Si coordinations. Samples with phase-separated TiO_2 and ZrO_2 would exhibit further resonances at typically 360 ppm, assigned to a mixture of OTi_4 and OZr_3 sites, and at 530 ppm, assigned to OTi_3.[29]

2.8. XRD. XRD spectra were collected on a SX3000 Seifert diffractometer equipped with a lithium fluoride monochromator on the diffracted beam. The scans were collected in the range from 10° to 120° (2θ) by use of Cu Kα radiation ($\lambda = 1.545$ Å). Bragg peaks occur at approximately 30°, 50°, and 60° for t-ZrO_2 phase-separated domains[30] and at 30°, 54°, and 64° for $ZrTiO_4$ phase-separated domains.[31]

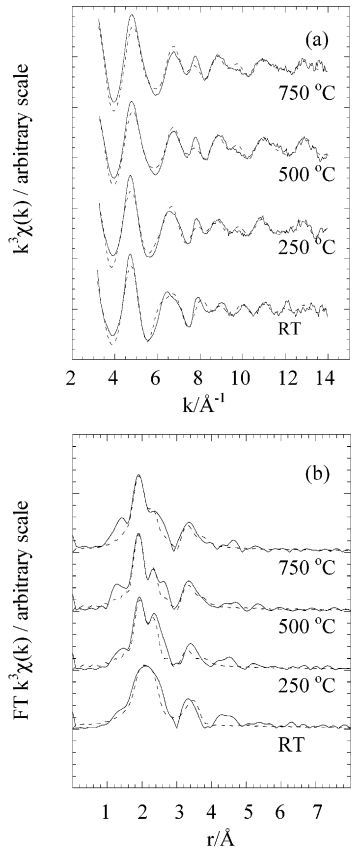

Figure 1. Zr K-edge EXAFS fits for Zr15/Ti5 ternary xerogel composition: (a) $k^3\chi(k)$ and (b) FT $k^3\chi(k)$.

3. Results

3.1. EXAFS. To aid in the interpretation of results, Table 1 describes the environments of Zr and Ti in various reference compounds. In general, there is good agreement between the crystallographic data and the corresponding EXAFS fits. Attempts to fit the $ZrTiO_4$ EXAFS data gave only partial success. This is most likely to be due to limitations in the published information about the crystal structure; in particular, the proposed site for Ti atoms seems very unrealistic, and the fit to the Ti K-edge data was not very good. The $NaZrO_3$ data was not fitted due to lack of information about the crystal structure.

Panels a and b, respectively, of Figure 1 show the experimental $k^3\chi(k)$ and the magnitude of the FT of $k^3\chi(k)$ from the Zr K-edge for the Zr15/Ti5 series of samples. The results from these fits and the remaining Zr K-edge data are summarized in Table 2. As in our previous work,[4,5] attempts were made to fit the EXAFS data with both single Zr−O shells and split Zr−O shells (where the best fit is considered in terms of the quality of fit in relation to the number of fitting parameters). The samples are best fitted with a structural model consisting of a split Zr−O shell and one Zr−Zr distance. This splitting of the Zr−O shell is similar to that observed in t-ZrO_2.[5] It has also been observed in EXAFS studies of Zr propoxides.[32] In our previous work,[5] this splitting corresponded to Zr that is homogeneously mixed in the silica network (for samples with phase-separated Zr, a single Zr−O shell gave a better fit). Attempts to include a Zr−Si shell gave a poorer fit, due to the weak backscattering nature of Si. For the room-temperature samples, a better fit is achieved with a Zr−C shell, which is attributed to a greater number of residual organic groups remaining in the nonheated samples (and accentuated by the use of acac in the sample preparation). The observed Zr−O distances generally decrease as the heat treatment temperature is increased, as observed in our previous work.[4,5]

TABLE 2: Zr K-Edge EXAFS Results for Fits to Ternary Xerogels[a]

	Zr K-edge EXAFS results[b]				
sample	shell	N_{R-O}	R_{R-O}/Å	$2\sigma^2$/Å^2	R_{dis}/%
Zr15/Ti5(RT)	Zr−O_a	2.4 (0.5)	2.08 (0.01)	0.013 (0.001)	
	Zr−O_b	3.2 (0.6)	2.23 (0.01)	0.015 (0.001)	
	Zr−C	4.3 (0.9)	3.47 (0.01)	0.007 (0.001)	
Zr15/Ti5(250)	Zr−O_a	1.5 (0.3)	2.04 (0.01)	0.005 (0.001)	34
	Zr−O_b	3.7 (0.7)	2.21 (0.01)	0.016 (0.001)	
	Zr−Zr	2.3 (0.5)	3.37 (0.02)	0.029 (0.002)	
Zr15/Ti5(500)	Zr−O_a	1.2 (0.2)	2.02 (0.01)	0.003 (0.001)	31
	Zr−O_b	4.0 (0.8)	2.17 (0.01)	0.023 (0.001)	
	Zr−Zr	3.0 (0.6)	3.37 (0.02)	0.029 (0.002)	
Zr15/Ti5(750)	Zr−O_a	1.7 (0.3)	2.01 (0.01)	0.009 (0.001)	34
	Zr−O_b	4.7 (0.9)	2.18 (0.01)	0.028 (0.001)	
	Zr−Zr	1.0 (0.2)	3.35 (0.02)	0.007 (0.002)	
Zr10/Ti10(RT)	Zr−O_a	2.2 (0.4)	2.02 (0.01)	0.009 (0.001)	31
	Zr−O_b	4.6 (0.9)	2.21 (0.01)	0.019 (0.001)	
	Zr−C	6.1 (1.2)	3.48 (0.02)	0.010 (0.002)	
Zr5/Ti5(RT)	Zr−O_a	1.5 (0.3)	2.02 (0.01)	0.005 (0.001)	37
	Zr−O_b	4.8 (1.0)	2.25 (0.01)	0.025 (0.001)	
	Zr−C	5.3 (1.0)	3.51 (0.02)	0.004 (0.002)	
Zr5/Ti10(RT)	Zr−O_a	1.8 (0.5)	2.03 (0.01)	0.007 (0.001)	34
	Zr−O_b	3.3 (0.5)	2.25 (0.01)	0.018 (0.001)	
	Zr−C	6.2 (1.2)	3.51 (0.02)	0.007 (0.002)	
Zr5/Ti15(RT)	Zr−O_a	1.2 (0.2)	2.01 (0.01)	0.005 (0.001)	36
	Zr−O_b	5.4 (1.1)	2.21 (0.01)	0.026 (0.001)	
	Zr−C	3.2 (0.6)	3.52 (0.02)	0.010 (0.002)	
Zr5/Ti15(250)	Zr−O_a	1.5 (0.3)	2.07 (0.01)	0.009 (0.001)	38
	Zr−O_b	2.9 (0.6)	2.23 (0.01)	0.015 (0.001)	
	Zr−Zr	1.2 (0.2)	3.36 (0.02)	0.020 (0.002)	
Zr5/Ti15(500)	Zr−O_a	1.2 (0.2)	2.03 (0.01)	0.007 (0.001)	34
	Zr−O_b	3.6 (0.7)	2.21 (0.01)	0.029 (0.001)	
	Zr−Zr	1.6 (0.3)	3.36 (0.02)	0.025 (0.002)	
Zr5/Ti15(750)	Zr−O_a	2.1 (0.4)	2.07 (0.01)	0.013 (0.001)	31
	Zr−O_b	3.0 (0.6)	2.22 (0.01)	0.016 (0.001)	
	Zr−Zr	2.0 (0.4)	3.40 (0.02)	0.026 (0.002)	

[a] Errors are shown in parentheses. R_{dis} is the "goodness of fit", defined in eq 2. [b] k range = 3.6−13 Å^{-1}.

Panels a and b, respectively, of Figure 2 show the experimental $k^3\chi(k)$ and the magnitude of the FT of $k^3\chi(k)$ from the Ti K-edge for the Zr5/Ti15 series of samples, respectively. The structural parameters derived from these EXAFS fits are reported in Table 3. The Ti K-edge data is best fitted with a structural model consisting of a single Ti−O distance and second shells of Ti−C and Ti−Si for the nonheated and heated samples, respectively. In our previous work on $(TiO_2)_x(SiO_2)_{1-x}$ xerogels, a Ti−C correlation was observed in nonheated samples when acac was used in the preparation.[6] Once again, the observed Ti−O distances are similar to those observed in our previous work and also display similar trends in the variation of the Ti−O distance (decreasing from 1.86 to 1.82 Å) as the heat treatment temperature is increased.[6,7]

3.2. XANES. Figure 3a shows the XANES spectra for the reference compounds for the Zr K-edge data. A double peak is observed for $ZrSiO_4$ and t-ZrO_2 corresponding to ZrO_8 sites, and a single peak for sites with 7-fold coordination without Zr−O splitting is seen for m-ZrO_2. The results for $BaZrO_3$ and $ZrTiO_4$ represent Zr with octahedral coordination.

Panels b−d in Figure 3 display the XANES preedge peaks for the ternary samples. It can be seen for the samples with various Ti and Zr compositions (Figure 3b) that the shape of the preedge hardly changes with composition, implying little change in local environment of Zr as a function of metal content. The Zr15/Ti5 series of samples (Figure 3c) show changes with heat treatment that are consistent with those previously observed

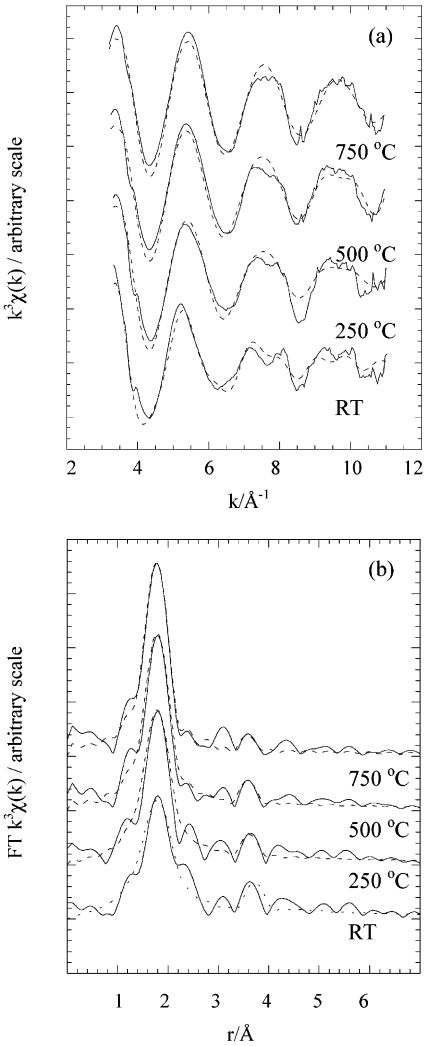

Figure 2. Ti K-edge EXAFS fits for Zr5/Ti15 ternary xerogel composition: (a) $k^3\chi(k)$ and (b) FT $k^3\chi(k)$.

for ZrO_2–SiO_2 xerogels with 15 mol % ZrO_2, in which Zr was found to be homogeneously distributed in the silica network.[5] An interesting exception is seen in the Zr5/Ti15 series of samples (Figure 3d). These are initially similar to the other samples, but after heat treatment at 750 °C the main absorption edge develops a negative slope at the top of the absorption edge (see asterisk) that is not observed for any of the other samples. Other complementary techniques (e.g., SAXS and XRD) have been used to further assess the significance of this XANES result and are addressed later on in this work.

Figure 4a shows the XANES results for the Ti K-edge reference samples; they are consistent with the known regular and distorted 6-fold Ti in reference compounds anatase and $ZrTiO_4$, respectively. Figure 4b displays the Ti K-edge XANES results for all of the nonheated xerogels. As can be seen, the preedge features are very similar for all compositions, inferring that Ti is present in the same configuration for all nonheated compositions, in agreement with the Ti K-edge EXAFS results. Panels c and d of Figure 4 show the XANES spectra for the Zr15/Ti5 and Zr5/Ti15 series of samples, respectively. There is a clear change in position and height of the dominant preedge peak. The height of the preedge peak increases sequentially as Ti coordination changes from 6- to 5- to 4-fold, due to decreasing centrosymmetry as the coordination changes from octahedral to square pyramidal to tetrahedral, respectively.[14,15] Hence the results in Figure 4c,d correspond to a decrease in Ti coordination with heat treatment. Very similar results were observed in our previous study of TiO_2–SiO_2 xerogels with 18 mol % TiO_2, in which Ti is homogeneously distributed in the silica network.[7,16] In that case the coordination of Ti changes from 6- to 4-fold with heat treatment due to loss of water (and alcohol) ligands.

TABLE 3: Ti K-Edge EXAFS Results for Fits to Ternary Xerogels[a]

	Ti K-edge EXAFS results[b]				
sample	shell	N_{R-O}	R_{R-O}/Å	$2\sigma^2$/Å^2	R_{dis}/%
Zr15/Ti5(RT)	Ti−O	6.2 (1.2)	1.85 (0.01)	0.031 (0.001)	33
	Ti−C	5.9 (1.2)	3.71 (0.02)	0.010[c]	
Zr15/Ti5(250)	Ti−O	3.9 (0.8)	1.82 (0.01)	0.020 (0.001)	33
	Ti−Si	0.3 (0.1)	3.12 (0.02)	0.010[c]	
Zr15/Ti5(500)	Ti−O	3.6 (0.7)	1.84 (0.01)	0.011 (0.001)	33
	Ti−Si	0.5 (0.1)	3.17 (0.02)	0.010[c]	
Zr15/Ti5(750)	Ti−O	4.4 (0.9)	1.79 (0.01)	0.012 (0.001)	36
	Ti−Si	0.4 (0.1)	3.14 (0.02)	0.010[c]	
Zr10/Ti10(RT)	Ti−O	4.4 (0.9)	1.86 (0.01)	0.026 (0.001)	35
	Ti−C	5.9 (1.2)	3.73 (0.02)	0.010[c]	
Zr5/Ti5(RT)	Ti−O	4.1 (0.8)	1.84 (0.01)	0.019 (0.001)	34
	Ti−C	5.9 (1.2)	3.72 (0.02)	0.010[c]	
Zr5/Ti10(RT)	Ti−O	4.1 (0.8)	1.83 (0.01)	0.020 (0.001)	34
	Ti−C	5.6 (1.1)	3.71 (0.02)	0.010[c]	
Zr5/Ti15 (RT)	Ti−O	5.2 (1.0)	1.86 (0.01)	0.030 (0.001)	31
	Ti−C	4.9 (1.0)	3.72 (0.02)	0.010[c]	
Zr5/Ti15 (250)	Ti−O	3.7 (0.7)	1.84 (0.01)	0.013 (0.001)	26
	Ti−Si	0.6 (0.1)	3.14 (0.02)	0.010[c]	
Zr5/Ti15 (500)	Ti−O	3.6 (0.7)	1.83 (0.01)	0.011 (0.001)	24
	Ti−Si	0.3 (0.1)	3.17 (0.02)	0.010[c]	
Zr5/Ti15 (750)	Ti−O	3.6 (0.7)	1.82 (0.01)	0.010 (0.001)	20
	Ti−Si	0.7 (0.1)	3.17 (0.02)	0.010[c]	

[a] Errors are shown in parentheses. R_{dis} is the "goodness of fit", defined in eq 2. [b] k range = 3.6−11 Å^{-1}. [c] Fixed fitting parameter.

3.3. SAXS. Figure 5 shows the SAXS plots for the Zr15/Ti5, Zr10/Ti10, and Zr5/Ti15 samples before and after heat treatment at 750 °C. By reference to previous work,[17] the scattering from the xerogels can be attributed to two main sources. First, the plots are dominated by a large negative slope at low Q values (0.01−0.05 Å^{-1}). This is caused by the surface roughness of the xerogel samples associated with the micropores that permeate the silica-based network. Second, and most importantly, inhomogeneities can exist in the samples in the form of phase-separated regions. If such phase-separated domains are present in these samples, a shoulder appears in the scattering curve at higher Q values (∼0.1 Å^{-1}), and the position of the shoulder can be used to estimate the size of the domains.[17] The SAXS results for unheated samples do not show any significant features at high Q. The SAXS results for sample Zr5/Ti15(750) do show a distinct hump at $Q \sim 0.15$ Å^{-1}, which is evidence of phase-separated regions of size ∼1 nm.[17] In contrast, the SAXS results for Zr10/ Ti10(750) and Zr15/ Ti5(750) do not show clear signs of phase separation. This is consistent with Zr K-edge XANES results, which indicate a distinctive structure for the sample Zr5/Ti15(750).

3.4. FTIR. FTIR spectroscopy corroborates our other data in several respects but provides no qualitatively new information per se, and spectra are therefore not reproduced here. A band at 960 cm^{-1} is revealed for all sample compositions and heat treatments, which indicates atomic mixing of Ti and/or Zr into the silica lattice to form Ti−O−Zr and/or Ti−O−Si linkages. Also, convoluted into this band is the contribution from Si−(OH) stretches, which become less intense as the heat treatment temperature is increased for any given sample series due to the loss of −OH groups. Coupled to this observation is a decrease in intensity of bands observed at 3590 and 1610 cm^{-1}, which

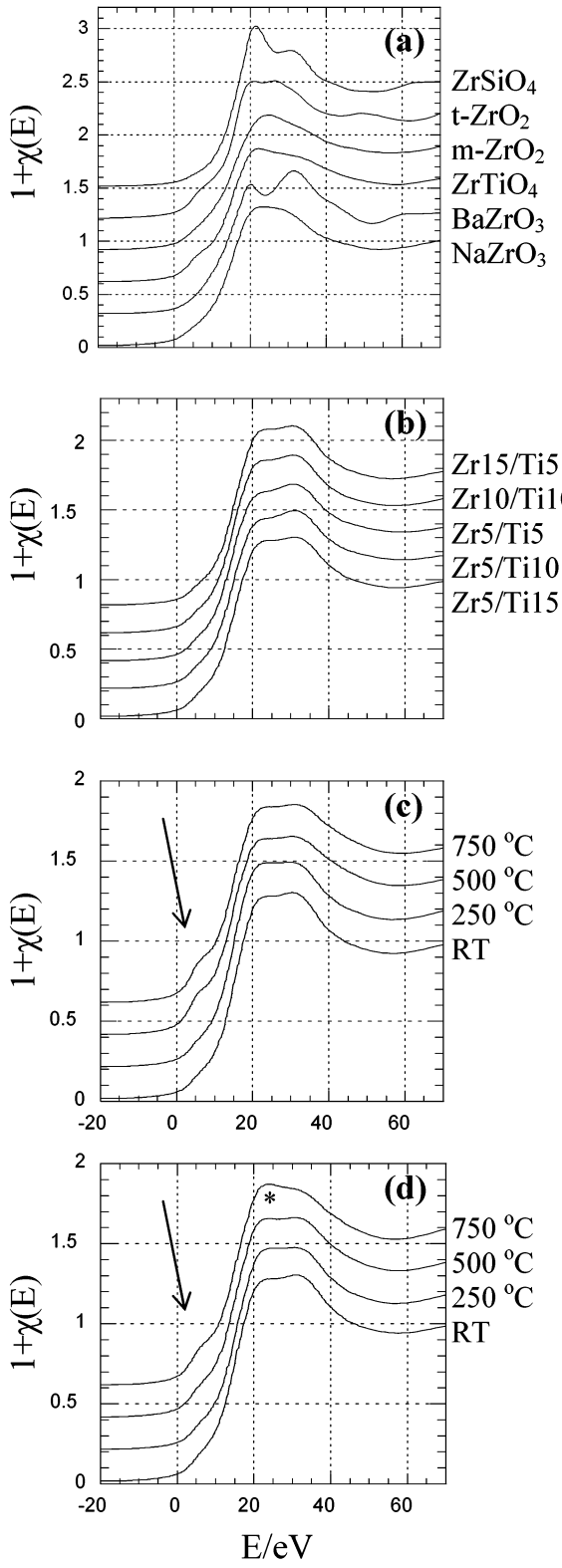

Figure 3. Zr K-edge XANES spectra for (a) reference compounds, (b) all nonheated xerogels, and (c) Zr15/Ti5 and (d) Zr5/Ti15 ternary xerogels with heat treatment. Arrows indicate the shoulder on the low-energy side of the edge. The asterisk indicates the negative slope at the top of the edge for Zr5/Ti15(750).

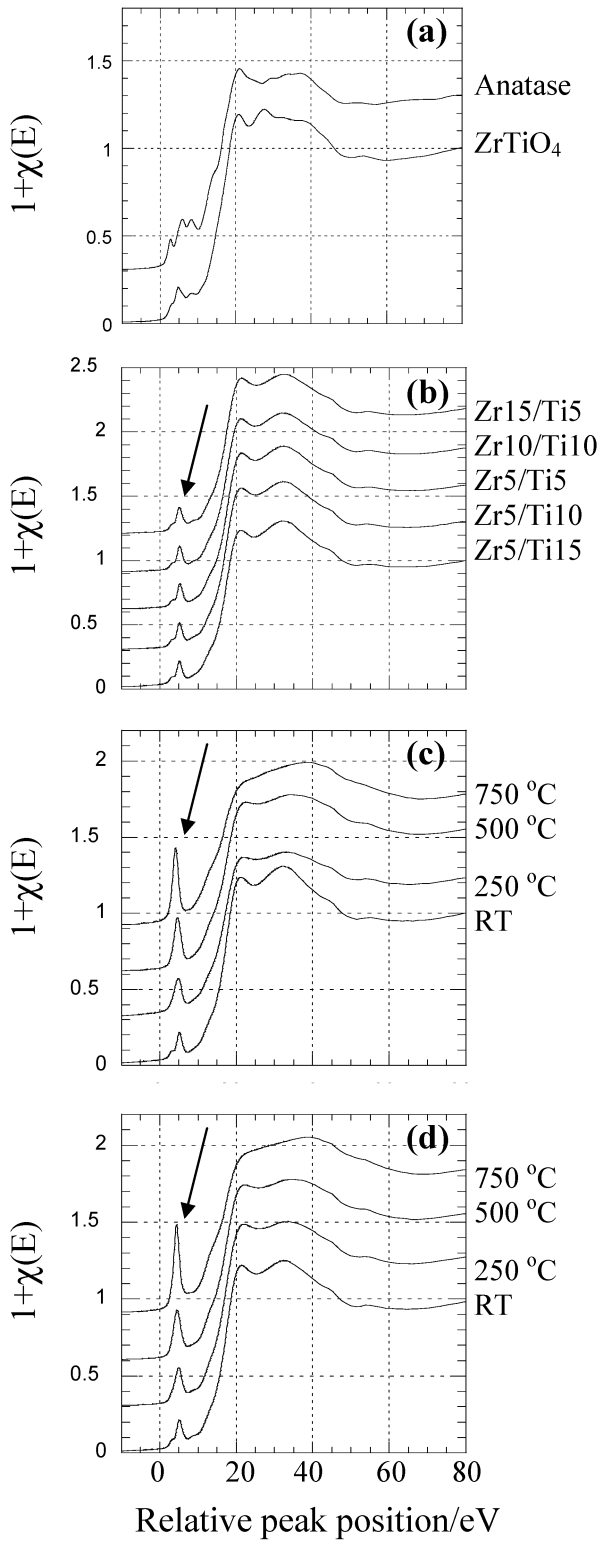

Figure 4. Ti K-edge XANES spectra for (a) reference compounds, (b) all nonheated xerogels, and (c) Zr15/Ti5 and (d) Zr5Ti15 ternary xerogels with heat treatment. The arrow indicates the preedge peak.

represent the loss of −(OH) and H−O−H groups as the temperature of the heat treatment is raised. The disappearance of sharp, weak bands at ca. 2900 and 1450 cm^{-1} and ca. 1600, 1530, 1360, and 1280 cm^{-1} with heat treatment at 250 °C provides evidence for the expected removal of organic materials.

3.5. ^{17}O MAS NMR. The ^{17}O MAS NMR spectra show that the Zr15/Ti5 samples (Figure 6a) are homogeneous up to 500 °C with a definite resonance at 180 ppm from M−O−Si. This peak is present in the 750 °C sample but also it shows some signs of phase separation (as inferred by the resonance at ∼350 ppm). The ^{17}O MAS NMR spectra for the Zr5/Ti15 samples (Figure 6b) show once again that the samples are homogeneous up to 500 °C. However, sample Zr5/Ti15(750) has a resonance

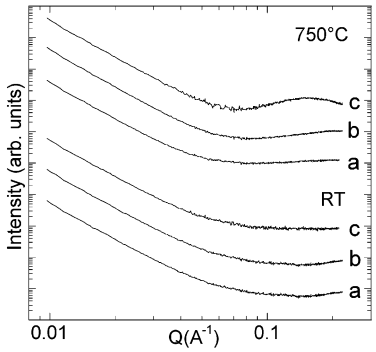

Figure 5. SAXS results for (a) Zr15/Ti5, (b) Zr10/Ti10, and (c) Zr5/Ti15 before and after heat treament at 750 °C.

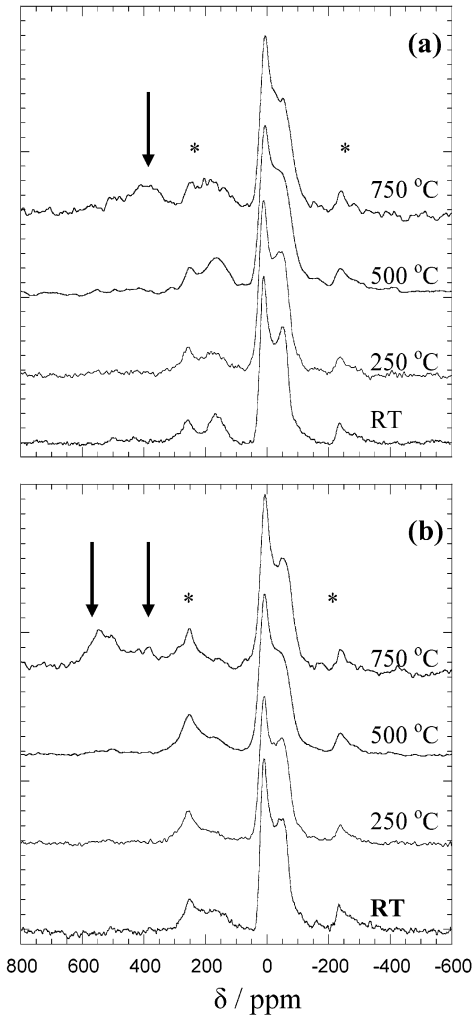

Figure 6. ^{17}O MAS NMR spectra for (a) Zr15/Ti5 and (b) Zr5/Ti15 ternary xerogel compositions with heat treatment. Asterisks denote spinning side bands. Arrows indicate features associated with phase separation in the form of OTi_3 and OZr_3.

at 530 ppm with broad intensity down to ∼350 ppm. It would appear straightforward to assign the 530 ppm resonance to phase separation in the form of OTi_3 from TiO_2. This then leads to an apparent discrepancy with the Zr K-edge XANES data, which suggest that the phase-separated regions in sample Zr5/Ti15(750) involve Zr. However, ^{17}O MAS NMR spectra from sol−gel-prepared crystalline $ZrTiO_4$ show a broad resonance extending over 500−300 ppm.[33] Hence the ^{17}O NMR spectrum from Zr5/Ti15(750) could contain contributions from some TiO_2 but also significant amounts of $ZrTiO_4$. Note that NMR is a short-range

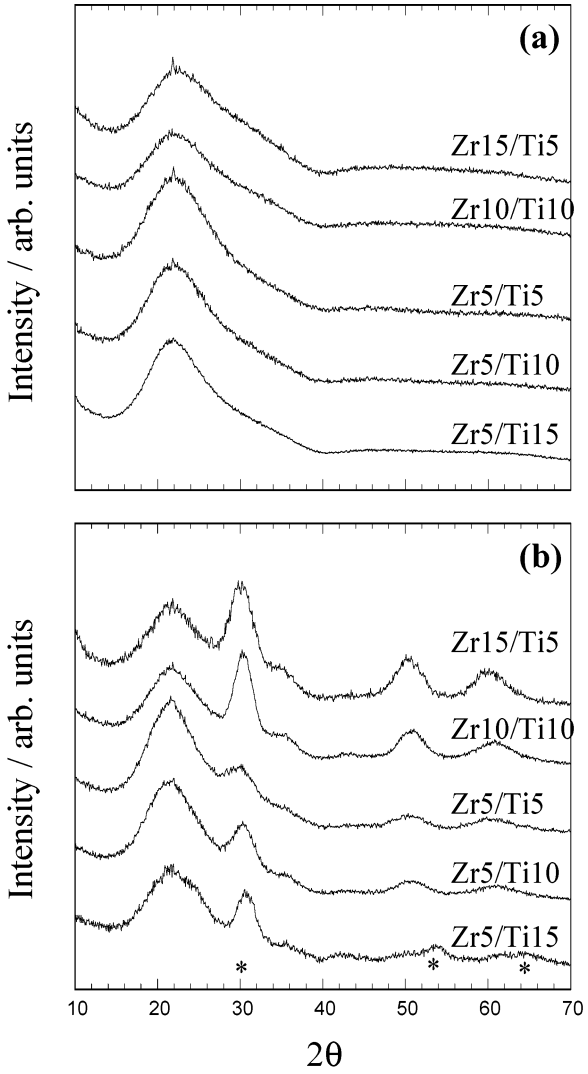

Figure 7. Cu Kα XRD spectra for all ternary xerogels after heat treatment at (a) 750 and (b) 1000 °C. Asterisks indicate Bragg peaks due to $ZrTiO_4$.

technique, being sensitive to local electron density. For a measurable M−O−M signal, i.e., local electron density similar to that in a metal oxide, the phase-separated region has to be at least several M−O−M bonds in diameter.

3.6. XRD. XRD showed that the samples are amorphous after heat treatment at 750 °C (Figure 7a). Additional heat treatment was carried out solely for the purpose of investigating crystallization of metal oxide phases. Results after heat treatment to 1000 °C (Figure 7b) show crystallization of t-ZrO_2 phase[30] in all samples except for Zr5/Ti15(1000). In this sample a $ZrTiO_4$ phase[31] has crystallized (see asterisks). The breadth of the Bragg peaks indicates very small crystal domains, but quantitative estimates of crystal size were not obtained.

4. Discussion

4.1. Structural Changes as a Function of Heat Treatment. On considering the Ti K-edge EXAFS data, one observes large Debye−Waller factors for the unheated samples. This is most likely to be caused by a proportion of the Ti being complexed by acac (acetylacetone) ligands and thus increasing the static disorder. This implies distorted octahedral geometry ($N_{R-O} \sim 6$). The most likely distortion is two short Ti−(OSi) bonds and four longer Ti−acac bonds. This configuration has also been observed in previous EXAFS[6] and XANES[7] on unheated TiO_2−

SiO_2 xerogels prepared with acac. The Ti K-edge data for the unheated Zr5/Ti15(RT) and Zr15/Ti5(RT) samples gives an average $R_{Ti-O} = 1.86$ Å, which is intermediate between the mean Ti−O distances of 1.80 and 1.96 Å expected for 4- and 6-fold coordination, respectively. Note that Ti with distorted 6-fold coordination has both short and long Ti−O bonds, and fitting a single Ti−O shell to the EXAFS data produces a large Debye−Waller factor and a mean Ti−O distance that is dominated by the short Ti−O bonds, as seen in our previous work.[7] This contrasts with EXAFS results for Ti with regular 6-fold coordination (see results for anatase in Table 1). (The fitted coordination number is lower than 6, but we recall that the EXAFS technique is only able to determine nearest-neighbor coordinations with precision of the order ±20%.)

Heat treatment of the Zr5/Ti15 and Zr15/Ti5 series of xerogels up to 750 °C causes small but significant changes in the EXAFS results (as displayed in Table 3). There is a slight decrease in the R_{Ti-O} and N_{Ti-O} values, which suggests that the percentage of Ti in a 4-fold configuration is becoming more prevalent with heat treatment. In addition, the Debye−Waller factor and the fit index, R_{dis}, decrease with heat treatment, suggesting the formation of a more ordered Ti−O correlation for both compositions. The relatively low Debye−Waller factors of 0.09 and 0.011 Å^2 for the Zr5/Ti15(750) and Zr15/Ti5(750) xerogel Ti−O shells is an indication that nearly all of the Ti is located in one environment (i.e., the static disorder is relatively small). Similar trends have been seen previously in work that highlighted the effects of heat treatment on Ti coordination in TiO_2−SiO_2 xerogels.[7]

The Ti K-edge XANES spectra support the EXAFS data in showing an increase in intensity of the preedge features (as shown in Figure 4c,d) from mostly 6-fold through to a mixture of 4- and 6-fold, with the majority being 4-fold by 750 °C. This change in coordination is attributed to Ti that is homogeneously mixed in the silica network and hence adopts 4-fold coordination upon the removal of residual water and alcohol ligands caused by heat treatment.

The Zr K-edge EXAFS results show a splitting of the Zr−O shell for all the unheated samples, with a mean $R_{Zr-O} = 2.17$ Å and $N_{Zr-O} = 6.1$ (see Table 2). The mean Zr−O distance suggests a Zr local environment with 7-fold coordination with respect to oxygen. Zr with 7-fold coordination and a split Zr−O shell is found in cubic ZrO_2.[36] However, this observation should be treated with caution given that cubic ZrO_2 contains only O−Zr$_n$ configurations, which have not been observed in EXAFS or other techniques. The Zr K-edge XANES spectra for the Zr15/Ti5(RT) and Zr5/Ti15(RT) samples (as shown in Figure 3, panels c and d, respectively) are very similar in shape to that seen in Zr *n*-propoxide,[5] but the EXAFS results here give R_{Zr-Oa} and R_{Zr-Ob} longer than those for Zr *n*-propoxide. Hence, from the Zr EXAFS and XANES data we propose a Zr environment similar to that seen in Zr propoxide but with coordination of 7 rather than 6.

After heat treatment of the Zr15/Ti5 and Zr5/Ti15 series of xerogels, the Zr K-edge EXAFS data follow the pattern previously seen for ZrO_2−SiO_2 xerogels in which the Zr is homogeneously mixed.[5] The general trend is a reduction in values of *N* and *R* as heat treatment is increased. Hence, one may assume that the effect of increasing the heat treatment is to cause a reduction in the average Zr−O coordination number, similar to the Ti case, primarily due to the loss of water and alcohol ligands. In particular, both Zr15/Ti5 and Zr5/Ti15 show a decrease in N_{Zr-Oa}, R_{Zr-Oa}, R_{Zr-Ob}, and A_{Zr-Oa} as heat treatment goes from 250 to 500 °C. For Zr15/Ti5 these values remain small at 750 °C, but for Zr5/Ti15 there is a significant increase in the distance R_{Zr-Oa}. The anomalous behavior of this sample is addressed more fully in section 4.3.

The Zr K-edge XANES results complement this observation by showing the development of a slight shoulder on the low-energy side of the preedge (see arrow in Figure 3c,d), coupled with a subtle change of slope at the top of the absorption edge, as the heat treatment temperature is increased. The pronounced increase in overall intensity of the preedge shoulder has been observed in other studies of ZrO_2−SiO_2 xerogels that contain Zr homogeneously mixed into the silica lattice.[5]

FTIR spectroscopy confirms the generic structural changes that occur due to heating. The spectra for the unheated xerogels (all compositions) are dominated by vibrations caused by acac ligands and hydroxyl groups.[6] The intensity of the spectral features associated with these rapidly diminishes as the temperature of heat treatment reaches 500 °C, and they have vanished from the spectra by 750 °C, confirming removal of organic fragments. This has been observed in previous studies.[6]

4.2. Structural Changes as a Function of Composition. The Ti K-edge EXAFS results (see Table 3) show that the Debye−Waller factors are highest for the unheated samples that contain 20 mol % total metal loading (i.e., the highest levels). This is attributed to the distorted octahedral geometry that surrounds the Ti sites, as explained in section 4.1. The N_{Ti-O} value for the unheated samples is between 4 and 6, but the more reliably determined R_{Ti-O} values of 1.84−1.86 Å confirm the presence of a significant proportion of distorted 6-fold Ti. Hence, the Ti remains in a similar environment regardless of composition. The Zr K-edge EXAFS data for the unheated samples (see Table 2) give a similar result for the Zr environment as a function of composition. These show that the R_{Zr-Oa} and R_{Zr-Ob} distances fluctuate from 2.06 to 2.08 Å and 2.21 to 2.25 Å, respectively, which is insufficient to represent significant structural differences.

The Zr K-edge XANES spectra for the unheated samples (Figure 3b) display almost identical preedge features for all compositions. This result is in agreement with the Zr K-edge EXAFS results. Similarly, the Ti K-edge XANES spectra (Figure 4b) agree with the Ti K-edge EXAFS results, showing almost identical preedge features for all unheated compositions. These observations imply that in the unheated samples both Zr and Ti adopt similar configurations regardless of their concentration in the silica lattice. As the heat treatment temperature is increased, the XANES data only shows one clear difference between compositions. That is for the Zr5/Ti15(750) sample, which has a Zr K-edge XANES spectra clearly different from any other samples. Note, however, that the Ti K-edge spectrum is not different for this sample compared to other samples heat-treated at 750 °C. These results are addressed more fully in section 4.3.

The ^{17}O MAS NMR from the Zr5/Ti15 and Zr15/Ti5 series of samples may usefully be compared in order to elucidate the effect of the two different metal ions on the material. The spectra indicate that both these xerogels are atomically mixed since both have a peak at ∼180 ppm due to M−O−Si. This M−O−Si signal is much broader in the Zr5/Ti15 case, suggesting a larger distribution in the range of these environments than for Zr15/Ti5. On heating, the Zr15/Ti5 sample shows a higher degree of direct M−O−Si bonding, and there is lower intensity in the >350 ppm range, the latter only appearing after heating to 750 °C. In contrast the Zr5/Ti15 sample shows a significant reduction in intensity in the 200−150 ppm region and more intensity between 500 and 350 ppm. The implication is that

there is more phase separation in the Zr5/Ti15 sample. In the present work, the analysis of relative intensities of the peaks in ^{17}O NMR spectra remains qualitative rather than quantitative. It is estimated that approximately 10% of the oxygen is in the phase-separated region.

This conclusion is further reinforced by the SAXS data (Figure 5), which show no discernible phase separation for the Zr15/Ti5 xerogel. In contrast, the Zr5/Ti15 sample shows evidence of phase separation starting to occur at 750 °C. This is inferred from the distinct hump in the scattering curve at $Q \sim 0.15$ Å^{-1}. In a previous SAXS study,[17] similar features in the scattering curve were observed for $(TiO_2)_{0.18}(SiO_2)_{0.82}$ and $(ZrO_2)_{0.23}(SiO_2)_{0.77}$ xerogels heated to 750 °C, which were known to be phase-separated. Hence the SAXS data confirms that for heat treatments at higher temperatures, the modification of the silica network is most substantial in the Zr5/Ti15 sample.

4.3. Homogeneity/Phase Separation Effects. The as-prepared xerogels were manufactured by the sol−gel route to facilitate preparation of homogeneous glass products.[2,8] During the synthesis, especially at the stage of mixing the metal precursors and TEOS, no evidence was seen of any precipitation/turbidity in the sol, allowing the conclusion that the precursors were indeed well mixed.

As stated in section 4.1, the Zr K-edge XANES showed preedge features very similar to those observed in a previous study on ZrO_2-SiO_2 xerogels,[5] which showed Zr to be homogeneously incorporated into the silica lattice with loadings up to 15 mol %. That work also showed that ZrO_2-SiO_2 xerogels with high Zr loadings[5] (30−40 mol %) exhibited a XANES spectrum similar to that for m-ZrO_2. Xerogels with high Zr loadings were found to have phase-separated regions of ZrO_2 that were initially amorphous, with local atomic environments similar to m-ZrO_2, and that crystallized into t-ZrO_2 after heat treatment at higher temperatures.[5] In the XANES spectra for the current ternary samples, one abnormality is observed for sample Zr5/Ti15(750), which shows a distinct change in slope at the top of the preedge feature (marked with an asterisk in Figure 3d). By comparison with Figure 3a, this anomalous spectrum is seen to be more similar to that for $ZrTiO_4$ rather than m-ZrO_2. The Ti K-edge XANES results show no evidence of a substantial fraction of Ti involved in phase separation occurring for any of the samples, including Zr5/Ti15(750). This can be reconciled by considering that only a minor fraction of the total Ti in the Zr5/Ti15 sample would be involved in a $ZrTiO_4$ phase. The Zr and Ti K-edge XANES results taken together indicate the presence of $ZrTiO_4$, and not TiO_2, phase-separated regions.

The XRD results further support this conclusion. By referring to Figure 7 and the discussion in section 3.6, it is apparent that for all xerogel compositions heated to 1000 °C crystallization has occurred. The position of these peaks allows one to determine the type of crystallites present: the Zr5/Ti15(1000) xerogel is the only sample to show peaks corresponding to crystalline $ZrTiO_4$ domains (at $2\theta = 30°$, 54°, and 64°). At a heat treatment temperature of 750 °C the sample is X-ray amorphous, suggesting that the $ZrTiO_4$, although phase-separated from the bulk of the network, is nevertheless amorphous. The other xerogel compositions heated to 1000 °C show peaks corresponding to crystalline t-ZrO_2 domains (at $2\theta = 30°$, 50°, and 60°), which are observed most intensely for the Zr15/Ti5 sample.

From the ^{17}O MAS NMR data (Figure 6), it can be seen that the Zr5/Ti15(750) sample shows clear evidence of phase separation by the appearance of the two resonances at ca. 360 and 530 ppm and some broad intensity between. This may imply the detection of phase-separated regions of predominantly TiO_2, as indicated by other recent studies.[21] However, although there may be some TiO_2 present, the data are also consistent with the presence of $ZrTiO_4$. This emphasizes that, while phase separation may readily be detected per se in a ternary system of this nature, great care has to be exercised in the detailed interpretation of data, and it is highly advantageous to have available a range of complementary data. For the Zr15/Ti5(750) sample, the ^{17}O NMR spectra shows a definite resonance at ca. 360 ppm together with the absence of intensity above this region. This suggests that ZrO_2 is phase-separating and not TiO_2. This result is consistent with the XRD data, which show crystallization of t-ZrO_2 after heat treatment at 1000°C.

Previous studies have established the limits of homogeneity of binary TiO_2-SiO_2 and ZrO_2-SiO_2 xerogels. For $(TiO_2)_x(SiO_2)_{1-x}$[4,5,17] and $(ZrO_2)_x(SiO_2)_{1-x}$ xerogels[6,7,17] with $x \geq 0.2$, heat treatment causes the phase separation and eventual crystallization of a metal oxide. Phase separation in the ternary $ZrO_2-TiO_2-SiO_2$ systems has previously been studied by Wannagon et al.,[9] by using XRD to observe crystallization after heat treatment at up to 900 °C. Those results showed that, for high SiO_2 contents, one tends to get phase separation of $ZrTiO_4$ domains when there is more Ti than Zr but phase separation of ZrO_2 domains when there is more Zr than Ti. The data presented here are fully consistent with these previous findings.

Perhaps surprisingly, the Zr15Ti5(750) sample does not show such strong signs of phase separation as the Zr5Ti15(750) sample, even though it contains the same total metal content. A possible explanation for this is associated with the order in which the alkoxides were mixed into the silica sol during the preparation procedure. In the preparation method followed,[2,8] the Ti alkoxide was mixed with TEOS for about a minute prior to the Zr alkoxide, which may have affected the nature of the eventual Zr sites. For the Zr5Ti15 sample, a large amount of Ti alkoxide was added immediately prior to the Zr alkoxide, and this may have interfered with the process by which Zr is incorporated into the Si framework, laying the foundation for eventual phase separation of $ZrTiO_4$ domains.

5. Conclusions

The EXAFS and XANES results lead one to conclude that the simultaneous insertion of ≤15 mol % Ti and Zr oxides into a silica framework is associated with the metals adopting similar environments to those previously observed for the "binary" TiO_2-SiO_2 and ZrO_2-SiO_2 systems with similar amounts of metal oxide.[4,5,6,7,16] In addition, as the samples are heat-treated, the coordination of the Ti sites changes from predominantly 6-fold through a mixture of 4- and 6-fold to mostly 4-fold. Similarly, the Zr site coordination decreases as the heat treatment temperature is increased. This again follows the patterns seen in previous studies on single metal incorporation into a silica network.[4,5,6,7,16]

The EXAFS, XANES, and SAXS data imply a high degree of homogeneity for the samples that contain total metal loadings of ≤15 mol % for heat treatments up to 750 °C and of 20 mol % for heat treatments up to 500 °C. After heat treatment of 750 °C, Zr K-edge XANES, SAXS, and ^{17}O NMR results give evidence of phase separation of $ZrTiO_4$ domains in the sample containing high Ti content, i.e., Zr5Ti15. These domains of $ZrTiO_4$ are X-ray amorphous, but they crystallize with heat treatment at 1000 °C. The only evidence of phase separation in other samples heat-treated at 750 °C is ^{17}O NMR results for the high Zr content sample, i.e., Zr15Ti5, which indicate some

phase separation of ZrO_2. All the samples except Zr5Ti15 show some crystallization of ZrO_2 after heat treatment at 1000 °C.

Acknowledgment. We thank J. F. W. Mosslemans, N. Terrill, and L. M. Murphy for assisting with X-ray experiments and A. Corrias for collecting XRD measurements. We also thank the EPSRC for funding this work through Grants GR/N64267 and GR/ N64151 and via a Ph.D. studentship (M.A.H.).

References and Notes

(1) Makishama, A.; Ohashi, H.; Wakakawa, M.; Kotani, K.; Shimohira, T. *J. Non-Cryst. Solids* **1980**, *42*, 545.
(2) Beier, W.; Goktas, A. A.; Frischat, G. H. *J. Am. Ceram. Soc.* **1986**, *69*, C148.
(3) Yamane, M. In *Sol−Gel Technology for Thin Films, Fibres, Preforms, Electronics and Specialty Shapes*; Klein, L. C., Ed.; Noyes Publications: Park Ridge, NJ, 1988; p 200.
(4) Pickup, D. M.; Mountjoy, G.; Wallidge, G. W.; Newport, R. J.; Smith, M. E. *Phys. Chem. Chem. Phys.* **1999**, *1*, 2527.
(5) Mountjoy, G.; Pickup, D. M.; Anderson, R.; Wallidge, G. W.; Holland, M. A.; Newport, R. J.; Smith, M. E. *Phys. Chem. Chem. Phys.* **2000**, *2*, 2455.
(6) Pickup, D. M.; Mountjoy, G.; Wallidge, G. W.; Anderson, R.; Cole, J. M.; Newport, R. J.; Smith, M. E. *J. Mater. Chem.* **1999**, *9*, 1299.
(7) Mountjoy, G.; Pickup, D. M.; Wallidge, G. W.; Anderson, R.; Cole, J. M.; Newport, R. J.; Smith, M. E. *Chem. Mater.* **1999**, *11*, 1253.
(8) Wellbrock, U.; Beier, W.; Frischat, G. H. *J. Non-Cryst. Solids* **1992**, *147*, 350.
(9) Wannagon, A.; Mishima, N.; Wakasugi, T.; Ota R.; Fukunaga J. *J. Ceram. Soc. Jpn.* **1997**, *105*, 940.
(10) Filipponi, A. *J. Phys.*: *Condens. Mater.* **1995**, *7*, 9343.
(11) Wang W. C.; Chen, Y. *Phys. Stat. Sol. A.* **1998**, *168*, 351.
(12) Bianconi, A. In *X-ray Absorption*: *Principles and Applications and Techniques of EXAFS, SEXAFS and XANES*; Koninsberger, D. C., Prins, R., Eds.; John Wiley & Sons: New York, 1988; pp 573−662.
(13) Grunes, L. A. *Phys. Rev. B* **1983**, *27*, 2111.
(14) Farges, F.; Brown, G. E.; Navrotsky, A.; Gan, H.; Rehr, J. J. *Geochim. Cosmochim. Acta* **1996**, *60*, 3039.
(15) Farges, F.; Brown, G. E.; Navrotsky, A.; Gan, H.; Rehr, J. J. *Phys. Rev. B.* **1997**, *56*, 1807.
(16) Mountjoy, G.; Pickup, D. M.; Wallidge, G. W.; Cole, J. M.; Newport, R. J.; Smith, M. E. *Chem. Phys. Lett.* **1999**, *304*, 150.
(17) Mountjoy, G.; Rigden, J. S.; Anderson, R.; Wallidge, G. W.; Newport, R. J.; Smith, M. E. *J. Mater. Res.* **2000**, *15*, 1998.
(18) Brinker, C. J.; Scherer, G. W. *Sol−Gel Science*; Academic Press: San Diego, CA, 1990.
(19) Matos, M. C.; Ilharco, L. M.; Almeida, R. M. *J. Non-Cryst. Solids* **1992**, *147*, 232.
(20) Schraml-Marth, M.; Walther, K. L.; Wokaun, A.; Handy, B. E.; Baiker, A. *J. Non-Cryst. Solids* **1992**, *143*, 93.
(21) Gunawidjaja, P. N.; Holland, M. A.; Mountjoy, G.; Pickup, D. M.; Newport, R. J.; Smith, M. E. *Solid State NMR* **2003**, *23*, 88.
(22) Smith, M. E.; van Eck, E. R. H. *Prog. NMR Spectrosc.* **1999**, *34*, 159.
(23) Walter, T. M.; Turner, G. L.; Oldfield, E. *J. Magn. Reson.* **1988**, *76*, 106.
(24) Dirken, P. J.; Smith, M. E.; Whitfield, H. J. *J. Phys. Chem.* **1995**, *99*, 395.
(25) Kroeker, S.; Rice, D.; Stebbins, J. F. *Am. Mineral.* **2002**, *87*, 572.
(26) Bastow, T. J.; Botton, G. A.; Etheridge, J.; Smith, M. E.; Whitfield, H. J. *Acta Crystallogr. A* **1999**, *55*, 127.
(27) Gervais, C.; Babonneau, F.; Hoebbel, D.; Smith, M. E. *Solid State NMR* **2000**, *17*, 2.
(28) Dajda, N.; Dixon, J. M.; Smith, M. E.; Carthey, N.; Bishop, P. T. *Phys. Rev. B* **2003**, *67*, 024201.
(29) Bastow, T. J.; Moodie, A. F.; Smith, M. E.; Whitfield, H. J. *J. Mater. Chem.* **1993**, *3*, 697.
(30) Malek, J.; Benes, L.; Mitsuhashi, T. *Powder Diffraction* **1997**, *12*, 96.
(31) Siggel, A.; Jansen, M. *Z. Anorg. Allg. Chemie* **1990**, *582*, 93.
(32) Reinhohl, U.; Ertel, T. S.; Horner, W.; Weber, A.; Bertahnolli, H. *Ber. Bunsen-Ges. Phys. Chem.* **1998**, *102*, 144.
(33) Bastow, T. J.; Smith, M. E.; Whitfield, H. J. Unpublished work.
(34) Burdett, J. K.; Hughbanks, T.; Miller, G. J.; Richardson, J. W.; Smith, J. V. *J. Am. Chem. Soc.* **1987**, *109*, 3639.
(35) Hazen, R. M.; Finger, L. W. *Am. Mineral.* **1979**, *64*, 196.
(36) Li, P.; Chen, I.-W.; Penner-Hahn, J. E. *Phys. Rev. B* **1993**, *48*, 10063.
(37) Megaw, H. D. *Proc. R. Soc. London* **1946**, *58*, 133.